Swing Dynamics as Primal-Dual Algorithm for Optimal Load Control

Changhong Zhao, Ufuk Topcu, Steven Low
California Institute of Technology
Pasadena, California 91125–0001

Abstract

Frequency regulation and generation-load balancing are key issues in power transmission networks. Complementary to generation control, loads provide flexible and fast responsive sources for frequency regulation, and local frequency measurement capability of loads offers the opportunity of decentralized control. In this paper, we propose an optimal load control problem, which balances the load reduction (or increase) with the generation shortfall (or surplus), resynchronizes the bus frequencies, and minimizes a measure of aggregate disutility of participation in such a load control. We find that, a frequency-based load control coupled with the dynamics of swing equations and branch power flows serve as a distributed primal-dual algorithm to solve the optimal load control problem and its dual. Simulation shows that the proposed mechanism can restore frequency, balance load with generation and achieve the optimum of the load control problem within several seconds after a disturbance in generation. Through simulation, we also compare the performance of optimal load control with automatic generation control (AGC), and discuss the effect of their incorporation.

I. Introduction

To ensure reliable power transmission, system operators must regulate the generation and load so that they match each other. Otherwise, the system frequency may deviate from the nominal value. Frequency deviations, if not tightly controlled around zero, may bring instability to the power system, or even permanently damage the facilities. Therefore, frequency regulation and generation-load balancing are important issues in power transmission networks.

Traditional regulation efforts rely on generation side. Automatic generation control (AGC), which adjusts the setpoints of generators based on area frequency deviation and unscheduled cross-area power flow, is a good example [1][2]. However, relying solely on generation side may not be enough. Due to limited ramping rate, generators are suitable for minute-to-minute generation and load balancing, but may incur expensive wear-and-tear, high emissions and low thermal efficiency when responding to regulation signals at intervals of seconds [3][4]. Complementary to generators, controllable loads provide low cost and fast responsive sources for power system regulation.

This artical is a technical report supporting the paper with the same title in the *Proceedings of IEEE SmartGridComm*, Tainan City, Taiwan, November 2012.

Feasibility and efficieny of load control has been justified in several electricity markets. Long Island Power Authority (LIPA) developed LIPA*edge*, which provided 24.9 MW of demand reduction and 75 MW of spinning reserve by 23,400 loads [5]. ERCOT has 50% of its 2400 MW reserve provided by loads. PJM opened up the regulation market to participation by loads [3]. While most of the installed programs focused on direct manipulation of loads in a centralized scheme, an alternative strategy, decentralized load control via frequency measurement, has been studied broadly in literatures. Brooks *et al.* suggested that loads can sense and respond to frequency and provide regulation within 1 second [4]. Molina-Garcia *et al.* studied the aggregated response characteristics when individual loads are turned on/off as the frequency goes across certain regions [6]. Donnelly *et al.* developed proportional frequency feedback control of intelligent loads, and investigated the effect of distribution systems, the effect of discretized control, and the effect of time-delay of control actions, using a 16-generator transmission network simulation test bed [7]. Literature review shows that frequency-based load control does not rely much on the communication to the centralized grid operator, thus suitable for large-scale, decentralized deployment [6][7].

In this paper, we consider a electricity transmission network in steady state where the generator frequencies at different buses (or in different balancing authorities) are synchronized to the same nominal value and the mechanic power is balanced with the electric power at each bus. Suppose a small disturbance in generation occurs on an arbitrary subset of the buses. How should the frequency-insensitive, controllable loads in the network be reduced (or increased) in real time in a way that (i) balances the generation shortfall (or surplus), (ii) resynchronizes the bus frequencies, and (iii) minimizes a measure of aggregate disutility of participation in such a load control? We formalize these questions as an *optimal load control (OLC)* problem. The basic dynamic at each generation bus is described by swing equations that relate the imbalance between generation and load to the rate of frequency change. We assume the generation disturbance is small and the DC load flow model is reasonably accurate. Then, we develop a frequency-based load control mechanism where loads are controlled as the inversed marginal disutility function of locally measured frequency. As a result of reverse engineering, such a frequency-based load control coupled with the dynamics of swing equations and power flows serve as a distributed primal-dual algorithm to solve *OLC*. Simulation on a 16-generator test bed shows that the proposed mechanism can restore frequency, balance load with generation and achieve the optimum of *OLC* within several seconds after a disturbance in generation. Moreover, we compare the performance of the proposed mechanism with AGC, and show with simulation that adding the proposed mechanism can improve the transient performance of AGC.

The paper is organized as follows. Section II describes the dynamics of power networks and introduces the *optimal load control (OLC)* problem. Section III interprets how the frequency-based load control and swing dynamics serve as a primal-dual algorithm to solve *OLC* and its dual. Section IV provides the convergence analysis of the primal-dual algorithm. Section V shows simulation-based case studies. Finally, Section VI provides concluding remarks and casts interesting points of future work.

II. Problem formulation

Let $\mathbb{R}$ denote the set of real numbers and $\mathbb{C}$ denote the set of complex numbers. A variable without a subscript usually denotes a vector with appropriate components, e.g., $d := (d_l, l \in \mathcal{L}(j), j \in \mathcal{V})$, $\omega := (\omega_j, j \in \mathcal{V})$, $P := (P_{ij}, (i,j) \in \mathcal{E})$. For a vector $a = (a_1, \ldots, a_k)$, a_{-i} denotes $(a_1, \ldots, a_{i-1}, a_{i+1}, a_k)$. For a matrix A, A^T denotes its transpose. Let t denote the time instance, and $\dot{\omega}$ denote $\frac{d\omega}{dt}(t)$.

A. Transmission network model

The transmission network is described by a graph $\mathcal{G} = (\mathcal{V}, \mathcal{E})$ where $\mathcal{V} = \{1, \ldots, N\}$ is the set of buses and $\mathcal{E}$ is the set of transmission lines connecting the buses. We adopt the following assumptions [1]

- The lines $(i,j) \in \mathcal{E}$ are lossless and characterized by their reactance $\mathbf{i}x_{ij}$.
- The voltage magnitudes $|V_j|$ of buses $j \in \mathcal{V}$ are constant.
- Reactive power injections at the buses and reactive power flows on the lines are ignored.

We assume that $\mathcal{G}$ is directed, with an arbitrary orientation, so that if $(i,j) \in \mathcal{E}$, then $(j,i) \notin \mathcal{E}$. We use (i,j) and $i \to j$ interchangeably to denote a link in $\mathcal{E}$. We also assume without loss of generality that $\mathcal{G}$ is connected. To simplify notation, we assume all variables represent deviations from their nominal (operating) values and are in per unit.

The dynamics at bus j with a generator is modeled by the swing equation

$$M_j \dot{\omega}_j \quad = \quad P_j^m - P_j^e,$$

where ω_j is the frequency deviation from its nominal value, M_j is the inertia constant of the generator, P_j^m is the deviation in mechanic power injection to bus j from its nominal value, and P_j^e is the deviation in electric power from its nominal value. Each bus may have two types of loads, *frequency-sensitive* (e.g. motor-type) loads and *frequency-insensitive* (but controllable) loads. The total change $\hat{d}_j$ in frequency-sensitive loads at bus j as a function of the frequency deviation ω_j is $\hat{d}_j := D_j \omega_j$, where D_j is the damping constant. Let $\mathcal{L}(j)$ denote the set of frequency-insensitive loads on bus j, and $(d_l, l \in \mathcal{L}(j))$ denote the deviations of frequency-insensitive loads from their nominal values. Then the electric power P_j^e is the sum of all frequency-sensitive loads, frequency-insensitive loads, and power flows from bus j to other buses, written as

$$P_j^e \quad = \quad D_j \omega_j + \sum_{l \in \mathcal{L}(j)} d_l + \sum_{k: j \to k} P_{jk} - \sum_{i: i \to j} P_{ij}.$$

Here P_{ij} is the deviation of branch flow from bus i to bus j from its nominal value. Our goal is to control the frequency-insensitive loads d_l in response to disturbances P_j^m in generation(mechanic) power. The swing equation can thus be rewritten as

$$\dot{\omega}_j \quad = \quad -\frac{1}{M_j} \left(\sum_{l \in \mathcal{L}(j)} d_l + D_j \omega_j - P_j^m + P_j^{\text{out}} - P_j^{\text{in}} \right), \tag{1}$$

[1] These assumptions are similar to the standard DC approximation except that we do not assume the phase angle difference is small across each link.

where $P_j^{\text{out}} := \sum_{k:j\to k} P_{jk}$ and $P_j^{\text{in}} := \sum_{i:i\to j} P_{ij}$ are total branch power flows out and into bus j, respectively.

We assume that the branch flows P_{ij} follow the dynamics

$$\dot{P}_{ij} \quad = \quad B_{ij}\,\omega^0\,(\omega_i - \omega_j)\,, \tag{2}$$

where ω^0 is the common nominal frequency on which the per-unit convention is based, and

$$B_{ij} \quad := \quad \frac{|V_i||V_j|}{x_{ij}} \cos\left(\theta_i^0 - \theta_j^0\right) \tag{3}$$

is a constant related to nominal voltages of buses and line reactance. The dynamic model (2)–(3) is motivated in the following way. Let θ_j denote the phase angle deviations of the bus voltages, i.e., the voltage phasors are $V_j := |V_j| e^{j(\theta_j^0 + \theta_j)}$ with the nominal phase angles θ_j^0. Consider the deviations in branch flows P_{ij} when the deviations are small [1], [9, Chapter 11]:

$$P_{ij} \quad = \quad B_{ij}(\theta_i - \theta_j), \tag{4}$$

and $\dot{\theta}_j = \omega^0 \omega_j$, then we have (2). Note that, while the model (4) assumes that the differences $\theta_i - \theta_j$ of the deviations are small, it does not assume the differences $\theta_i^0 - \theta_j^0$ of their nominal values are small.

In summary, the dynamic model of the transmission network is specified by (1)–(3). In steady state, the mechanic power deviations P_j^m are equal to the electric power deviations P_j^e, and $\omega_i = \omega_j$ for all the buses i and j, so $\dot{\omega}_j = 0$ and $\dot{P}_{ij} = 0$.

B. Optimal load control

Suppose a step change $P^m = (P_1^m, \ldots, P_N^m)$ in generation is injected to the N buses. How should the frequency-insensitive loads $d = (d_l, l \in \mathcal{L}(j), j \in \mathcal{V})$ in the network be reduced (or increased) in real-time in a way that (i) balances the generation shortfall (or surplus), (ii) resynchronizes the bus frequencies, and (iii) minimizes a measure of aggregate disutility of participation in such a load control? We now formalize these questions as an *optimal load control (OLC)* problem.

The disturbance P^m in generation causes a nonzero frequency deviation ω_j at bus j. This frequency deviation incurs a cost to frequency-sensitive loads and suppose this cost is $\frac{1}{2D_j}\hat{d}_j^2$ in total at bus j. Suppose the frequency-insensitive load $l \in \mathcal{L}(j)$ is to be changed by an amount d_l which incurs a cost (disutility) of $c_l(d_l)$. We assume $-\infty < \underline{d}_l \le d_l \le \overline{d}_l < \infty$. Our goal is to minimize the total cost over d and $\hat{d}$ while balancing generation and load across the network, written as

OLC

$$\min_{\underline{d} \le d \le \overline{d},\, \hat{d}} \qquad \sum_{j\in\mathcal{V}} \left(\sum_{l\in\mathcal{L}(j)} c_l(d_l) + \frac{1}{2D_j}\hat{d}_j^2 \right) \tag{5}$$

$$\text{subject to} \qquad \sum_{j\in\mathcal{V}} \left(\sum_{l\in\mathcal{L}(j)} d_l + \hat{d}_j \right) \quad = \quad \sum_{j\in\mathcal{V}} P_j^m. \tag{6}$$

Remark 1. Note that (6) does not require balance of generation and load at each individual bus, but only balance across the entire network. This constraint is less restrictive and offers more opportunity to minimize costs. Additional constraints can be imposed if it is desirable that certain buses balance their own supply and demand, e.g., for economic or regulatory reasons.

We assume the following condition throughout the paper:

C0: The *OLC* is feasible, and the cost functions c_l are strictly convex and twice continuously differentiable on $\left[\underline{d}_l, \overline{d}_l\right]$.

III. Load control and swing dynamics as primal-dual solution

In this section, we present our main results, whose proofs are in Section IV.

A. Key results

The objective function of the dual problem of *OLC* is:

$$\sum_{j\in\mathcal{V}} \Phi_j(\nu) \quad := \quad \sum_{j\in\mathcal{V}} \min_{\underline{d}_l \le d_l \le \overline{d}_l, \hat{d}_j} \left(\sum_{l\in\mathcal{L}(j)} (c_l(d_l) - \nu d_l) + \left(\frac{1}{2D_j} \hat{d}_j^2 - \nu \hat{d}_j \right) + \nu P_j^m \right),$$

where Φ_j can be written as

$$\Phi_j(\nu) \quad := \quad \sum_{l\in\mathcal{L}(j)} (c_l(d_l(\nu)) - \nu d_l(\nu)) - \frac{1}{2} D_j \nu^2 + \nu P_j^m, \tag{7}$$

with

$$d_l(\nu) \quad := \quad \left[c_l'^{-1}(\nu) \right]_{\underline{d}_l}^{\overline{d}_l}. \tag{8}$$

This objective function has a scalar variable ν and is not separable across buses $j = 1, \ldots, N$. Its direct solution hence requires coordination across the buses. We propose a following *distributed* version of the dual problem where each bus j optimizes over its own variable ν_j, one of the multiple copies of ν that are constrained to be equal at optimality.

DOLC

$$\begin{aligned} \max_{\nu_j} \quad & \Phi(\nu) := \sum_{j\in\mathcal{V}} \Phi_j(\nu_j) \\ \text{subject to} \quad & \nu_i = \nu_j \qquad \text{for all } (i,j) \in \mathcal{E}. \end{aligned}$$

Theorem 1. The following statements hold.

1) *DOLC* has a unique optimal solution ν^* with $\nu_i^* = \nu_j^* = \nu^*$ for all $i, j \in \mathcal{V}$.[2]
2) *OLC* has a unique optimal solution $(d^*, \hat{d}^*)$ where $d_l^* = d_l^*(\nu^*)$ is given by (8) for all $l \in \mathcal{L}(j)$, $j \in \mathcal{V}$, and $\hat{d}_j^* = D_j \nu^*$ for all $j \in \mathcal{V}$.

[2]We abuse notation and use ν^* to denote both the vector and the common value of its components.

3) There is no duality gap.

Instead of solving *OLC* directly, Theorem 1 suggests solving its dual *DOLC* and recovering the unique optimal solution $(d^*, \hat{d}^*)$ of the primal problem *OLC* from the unique dual optimal ν^*. To derive a distributed solution for *DOLC*, consider its Lagrangian

$$L(\nu, \pi) \quad := \quad \sum_{j \in \mathcal{V}} \Phi_j(\nu_j) - \sum_{(i,j) \in \mathcal{E}} \pi_{ij}(\nu_i - \nu_j), \tag{9}$$

where ν is the (vector) variable for *DOLC* and π is the associated dual variable for the dual of *DOLC*. Hence π_{ij}, for all $(i,j) \in \mathcal{E}$, measure the cost of not synchronizing the variables ν_i and ν_j across buses i and j. A primal-dual algorithm for *DOLC* takes the form (using (7)–(8))

$$\dot{\nu}_j \quad = \quad \gamma_j \frac{\partial L}{\partial \nu_j}(\nu, \pi) \;=\; -\gamma_j \left(\sum_{l \in \mathcal{L}(j)} d_l(\nu_j) + D_j \nu_j - P_j^m + \pi_j^{\text{out}} - \pi_j^{\text{in}} \right), \tag{10}$$

$$\dot{\pi}_{ij} \quad = \quad -\xi_{ij} \frac{\partial L}{\partial \pi_{ij}}(\nu, \pi) \;=\; \xi_{ij}(\nu_i - \nu_j), \tag{11}$$

where $\gamma_j > 0$, $\xi_{ij} > 0$ are stepsizes and $\pi_j^{\text{out}} := \sum_{k: j \to k} \pi_{jk}$, $\pi_j^{\text{in}} := \sum_{i: i \to j} \pi_{ij}$.

It is then remarkable that (10)–(11) become identical to (1)–(2), if we identify ν with frequency deviations and π with branch flows at every time instance t, i.e.,

$$\nu_j(t) = \omega_j(t), \qquad \pi_{ij}(t) = P_{ij}(t),$$

and the stepsizes γ_i and ξ_{ij} with the system parameters

$$\gamma_j = M_j^{-1}, \qquad \xi_{ij} = B_{ij} w^0.$$

For convenience, we collect the system dynamics and load control:

$$\dot{\omega}_j \quad = \quad -\frac{1}{M_j} \left(\sum_{l \in \mathcal{L}(j)} d_l + \hat{d}_j - P_j^m + P_j^{\text{out}} - P_j^{\text{in}} \right) \tag{12}$$

$$\dot{P}_{ij} \quad = \quad B_{ij}\, \omega^0 \, (\omega_i - \omega_j) \tag{13}$$

$$\hat{d}_j(\omega_j) \quad = \quad D_j \omega_j \tag{14}$$

$$d_l(\omega_j) \quad = \quad \left[c_l'^{-1}(\omega_j) \right]_{\underline{d}_l}^{\overline{d}_l} \qquad \text{for all } l \in \mathcal{L}(j), \tag{15}$$

where $P_j^{\text{out}} = \sum_{k: j \to k} P_{jk}$ and $P_j^{\text{in}} = \sum_{i: i \to j} P_{ij}$ are total branch power flows out and into bus j, ω^0 is the common nominal frequency, and B_{ij} are given by (3). The dynamics (12)–(14) are automatically carried out by the power system while the local control (15) need to be implemented at each frequency-insensitive load. Let $(d(t), \hat{d}(t), \omega(t), P(t))$ denote a trajectory of frequency-insensitive loads, frequency-sensitive loads, frequency deviations and power flows over time t, generated by the swing dynamics and the load control (12)–(15). We assume the following condition.

C1: For all $j \in \mathcal{V}$ and all $l \in \mathcal{L}(j)$, there exists some $\alpha_l > 0$ so that $c_l''(d_l) \geq 1/\alpha_l$ for $d_l \in \left[\underline{d}_l, \overline{d}_l\right]$. Moreover, $d_l'(\cdot) = \left((c_l')^{-1}\right)'(\cdot)$ is Lipschitz on $\left(c_l'\left(\underline{d}_l\right), c_l'\left(\overline{d}_l\right)\right)$.

Note that C1 is satisfied for disutility functions that are commonly used for demand response, e.g., quadratic function. With C1, we have the following theorem.

Theorem 2. Suppose the condition C1 is satisfied. Every trajectory $(d(t), \hat{d}(t), \omega(t), P(t))$ generated by (12)–(15) converges to a limit $(d^*, \hat{d}^*, \omega^*, P^*)$ as $t \to \infty$ such that

1) $(d^*, \hat{d}^*)$ is the unique vector of optimal load control for *OLC*;
2) ω^* is the unique vector of optimal frequency deviations for *DOLC*;
3) P^* is a vector of optimal branch flows for the dual of *DOLC*.

We will henceforth call a point $(d^*, \hat{d}^*, \omega^*, P^*)$ that satisfies the three conditions in Theorem 2 a *system optimal*.

B. Implications

Our results have several important implications:

1) *Frequency-based load control:* The frequency-insensitive loads can be controlled using their individual marginal cost functions according to (15), based only on frequency deviations $\omega_j(t)$ (from their nominal value) that are measured at their local buses.
2) *Complete decentralization.* The common operating frequency is a global signal that measures the power imbalance across the *entire* network. Our result implies that the local frequency deviation $\omega_j(t)$ at each bus turns out to convey exactly the right information about the global power imbalance for the loads themselves to make optimal decisions based on their own marginal cost functions. That is, with the right information, their local decisions turn out to be globally optimal. This allows a completely decentralized solution without the need for explicit communication among the buses.
3) *Reverse engineering of swing dynamics.* The frequency-based load control (15) coupled with the dynamics (12)–(14) of swing equations and branch power flows serve as a distributed primal-dual algorithm to solve *OLC* and its dual *DOLC*.
4) *Frequency and branch flows.* In the context of optimal load control, the frequency deviations $\omega_j(t)$ emerge as the Lagrange multipliers of *OLC* that measure the cost of power imbalance, whereas the branch flow deviations $P_{ij}(t)$ emerge as the Lagrange multipliers of *DOLC* that measures the cost of frequency asynchronism.
5) *Uniqueness of solution.* Theorem 1 implies that the optimal frequency ω^* is unique and hence the optimal load control $(d^*, \hat{d}^*)$ is unique. As we show below, the optimal branch flows P^* are unique if and only if the network is radial. Theorem 2 says nonetheless, that, even for mesh networks, any trajectory generated by the load control and swing dynamics indeed converges to an optimal point, with the optimal value of P^* dependent on the initial condition.
6) *Optimal frequency.* The structure of *DOLC* says that the frequencies at all the buses are synchronized at optimality even though they can be different during transient. Moreover, the common frequency *deviation* ω^* at optimality is in general nonzero. This fact implies that while frequency-based load control and the swing dynamics can resynchronize bus frequencies to a unique common value after a disturbance in generation,

the new frequency may be different from the nominal value (or the common operating frequency before the disturbance). Other mechanisms, such as automatic generation control, will be needed to drive the new operating frequency to its nominal value (e.g., 60Hz), through, e.g., intergal control over the frequency deviations.

Of course, many of these insights are well known; our results merely provide a fresh and unified interpretation within an optimization framework for frequency-based load control.

IV. Convergence analysis

Theorem 1, proved in the appendix Section VII-A, is simple since assumption C0 guarantees that *OLC* is a convex problem. This section is devoted to the proof of Theorem 2 and other properties. The main difficulty arises from the fact that optimal branch flows P^* may be nonunique. It takes a more sophisticated argument to show that $P(t)$ generated by the system (12)–(15) actually converges, as opposed to wandering around the set of optimal P^*.

We start by showing that the set of optimal solutions (ω^*, P^*) of *DOLC* and its dual, the set of saddle points of its Lagrangian, and the set of equilibrium points of (12)–(15) are all the same. Given $\omega(t)$, the optimal load $(d(t), \hat{d}(t))$ are uniquely determined by (14)–(15), so we will focus on $(\omega(t), P(t))$. For convenience, we rewrite (12)–(13) in vector form as follows. Recall the Lagrangian for *DOLC* defined in (9):

$$L(\omega, P) \quad = \quad \Phi(\omega) - \omega^T C P, \tag{16}$$

where C is the $N \times |\mathcal{E}|$ incidence matrix of $\mathcal{G}$, i.e., $C_{il} = 1$ if node i is the source of a directed link $l = (i, j)$, and $C_{il} = -1$ if node i is the sink of a directed link $l = (j, i)$. Then the system dynamics (12)–(13) are equivalent to

$$\dot{\omega}(t) \quad = \quad \Gamma \left[\frac{\partial L}{\partial \omega} \left(\omega(t), P(t) \right) \right]^T \;=\; \Gamma \left(\left[\frac{\partial \Phi}{\partial \omega} \left(\omega(t) \right) \right]^T - CP(t) \right), \tag{17}$$

$$\dot{P}(t) \quad = \quad -\Xi \left[\frac{\partial L}{\partial P} \left(\omega(t), P(t) \right) \right]^T \;=\; \Xi\, C^T \omega(t), \tag{18}$$

where $\Gamma = \text{diag}(\gamma_j)$ and $\Xi = \text{diag}(\xi_{ij})$.

The objective function $\Phi(\omega)$ of *DOLC* is (strictly) concave over $\mathbb{R}^N$ (proved in Lemma 1 in the appendix Section VII-A), its constraints are linear, and a finite optimal is attained. These facts imply that there is no duality gap between *DOLC* and its dual, and there exists a dual optimal solution P^* [10, Proposition 5.2.1], [11]. The Karush-Kuhn-Tucker conditions imply that (w^*, P^*) is optimal for *DOLC* and its dual if and only if

$$\frac{\partial \Phi}{\partial \omega}(\omega^*) \;=\; (CP^*)^T \quad \text{and} \quad w_i^* \;=\; w_j^* \quad \text{for all } i, j. \tag{19}$$

From (16), the conditions in (19) are also the first-order optimality conditions for $\min_\omega L(\omega, P^*)$ and $\max_P L(\omega^*, P)$ since $L(\omega, P)$ is (strictly) concave in ω and convex in P. Hence the KKT condition (19) implies that (ω^*, P^*) is primal-dual optimal if and only if it is a saddle point, i.e.,

$$L(\omega, P^*) \;\le\; L(\omega^*, P^*) \;\le\; L(\omega^*, P) \qquad \text{for all } (\omega, P). \tag{20}$$

Henceforth, we will refer to an (ω^*, P^*) as an optimal point of *DOLC* and its dual or as a saddle point of L interchangeably. Moreover, (w^*, P^*) is an equilibrium point of the system dynamics (17)–(18) if and only if

$$\frac{\partial L}{\partial \omega}(\omega^*, P^*) \;=\; 0 \quad \text{and} \quad \frac{\partial L}{\partial P}(\omega^*, P^*) \;=\; 0,$$

which is identical to the KKT condition (19). Hence (ω^*, P^*) is an equilibrium point if and only if it is a saddle point.

Denote the set of saddle/equilibrium points (ω^*, P^*) by $\mathcal{Z}^*$. By uniqueness of the optimal $\omega^* = (\omega^*, \ldots, \omega^*)^T$ of *DOLC* (Theorem 1), all points in $\mathcal{Z}^*$ have the same ω^*. Whether P^* is unique depends on the network topology.

Theorem 3. The following statements hold.

1) A point (ω^*, P^*) is an equilibrium point of (17)–(18) if and only if it is a saddle point of $L(\omega, P)$ (and hence optimal for *DOLC* and its dual). Moreover, such ω^* is unique.
2) If $\mathcal{G}$ is a tree, the equilibrium point (ω^*, P^*) is unique. Otherwise, the dynamics in (17)–(18) has an uncountably infinite number of equilibrium points with the same ω^* but different P^*.

Proof: The first assertion follows from the discussion preceding the theorem. Let $h(t) := CP(t)$. For the second assertion, any equilibrium point (ω^*, P^*) is a solution of (19) and $CP^* = h^* = \left[\frac{\partial \Phi}{\partial \omega}(\omega^*)\right]^T$. Let $\tilde{C}$ be the $(N-1) \times |\mathcal{E}|$ reduced incidence matrix obtained from C by removing (any) one of its rows. Then $\tilde{C}$ has a full row rank of $N-1$ [12]. Consider the corresponding equation

$$\tilde{C} P^* \;=\; \tilde{h}^*, \tag{21}$$

where $\tilde{h}^*$ is obtained from h^* by removing the corresponding row. Since ω^* is unique, so is $\tilde{h}^*$.

If $\mathcal{G}$ is a tree, then the number of lines $|\mathcal{E}| = N-1$. Hence $\tilde{C}$ is square and invertible, so P^* is unique. If $\mathcal{G}$ is a (connected) mesh, then $|\mathcal{E}| > N-1$ and, since $\tilde{C}$ is $(N-1) \times |\mathcal{E}|$, $\tilde{C}$ has a nontrivial null space and there are uncountably many P^* that solves (21). ■

We now study the stability of (17)–(18). Let $v := (\omega, P)$. Following [13], we consider the candidate Lyapunov function

$$U(v) = \frac{1}{2}\,(v - v^*)^T \begin{bmatrix} \Gamma^{-1} & 0 \\ 0 & \Xi^{-1} \end{bmatrix} (v - v^*) \tag{22}$$

where v^* is any equilibrium point of (17)–(18). Obviously $U(v) \geq 0$ for any v, with equality if and only if $v = v^*$. Moreover, for all $v \notin \mathcal{Z}^*$, the derivative of U along the dynamics (17)–(18) is

$$\begin{aligned} \dot{U}(v) \;&=\; (\omega - \omega^*)^T\,\Gamma^{-1}\dot{\omega} + (P - P^*)^T\,\Xi^{-1}\dot{P} \\ &=\; \frac{\partial L}{\partial \omega}(\omega, P)\,(\omega - \omega^*) - \frac{\partial L}{\partial P}(\omega, P)\,(P - P^*) && (23) \\ &\leq\; L(\omega, P) - L(\omega^*, P) + L(\omega, P^*) - L(\omega, P) && (24) \\ &=\; L(\omega, P^*) - L(\omega^*, P) \quad \leq \quad 0, \end{aligned}$$

where the first inequality follows because L is concave in ω and convex in P, and the last inequality follows from the saddle point condition (20). Hence U is indeed a Lyapunov function.

Let $E := \{v \mid \dot{U}(v) = 0\}$. Then, $v = (\omega, P) \in E$ if and only if $\omega = \omega^*$ (where ω^* is the unique optimal of *DOLC*). Indeed, note that if $\omega = \omega^*$, then the expression in (23) is zero since $\frac{\partial L}{\partial P}(\omega^*, P) = 0$ for any P. Conversely, if $\dot{U}(\omega, P) = 0$, then (24) must hold with equality. This is possible only if $\omega = \omega^*$ since L is *strictly* concave in ω and convex in P. Hence E has a simple characterization:

$$E \;=\; \{v \mid \dot{U}(v) = 0\} \;\;=\;\; \{(\omega, P) \mid \omega = \omega^*\}.$$

The set of saddle points is a strict subset of E, i.e., $Z^* \subsetneq E$, because if $(w^*, P) \in Z^*$ is a saddle point then P must satisfy $CP = \left[\frac{\partial \Phi}{\partial \omega}(\omega^*)\right]^T$ (from (19)). The sets E and Z^* are illustrated in Figure 1.

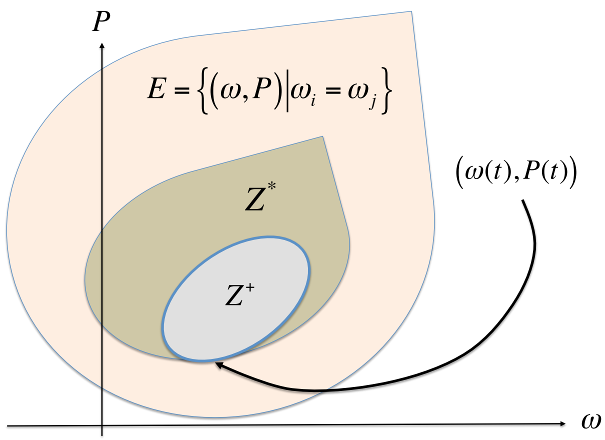

Fig. 1. E is the set on which $\dot{U} = 0$; $\mathcal{Z}^* = \{(\omega, P) | \frac{\partial \Phi}{\partial \omega}(\omega) = (CP)^T; \omega_i = \omega_j\}$ is the set of equilibrium/saddle/optimal points; $\mathcal{Z}^+$ is a compact subset of $\mathcal{Z}^*$ to which any solution $(\omega(t), P(t))$ approaches.

The set E contains points that are not optimal for *DOLC* and its dual (non-saddle points). Nonetheless, every accumulation point (limit point of any subsequence) of a solution $(\omega(t), P(t))$ of (17)–(18) is optimal, as the next result shows.

Theorem 4. Every solution $(\omega(t), P(t))$ of (17)–(18) approaches a nonempty, compact subset of $\mathcal{Z}^*$ as $t \to \infty$.

Proof: Note that the set $\{v | U(v) \le \alpha\}$ is compact and positively invariant with respect to (17)–(18) for any α. Hence, any solution $v(t)$ stays in the set $\{v | U(v) \le U(v(0))\}$ and remains bounded. LaSalle's invariance principle then implies that every solution $v(t)$ of (17)–(18) approaches the largest invariant set in E. Moreover the proof of LaSalle's invariance principle in [15, Theorem 3.4] shows that $v(t) = (\omega(t), P(t))$ approaches its positive limit set $\mathcal{Z}^+$ which is nonempty, compact, invariant, and a subset of E. We now show that $\mathcal{Z}^+ \subseteq \mathcal{Z}^* \subsetneq E$.

Consider any point $(\omega, P) \in \mathcal{Z}^+$. Since $\mathcal{Z}^+ \subseteq E$, we must have $\omega = \omega^*$, the unique optimal of *DOLC*. Moreover, since $\mathcal{Z}^+$ is invariant with respect to (17)–(18), a trajectory $(\omega(t), P(t))$ that starts in $\mathcal{Z}^+$ must stay in $\mathcal{Z}^+$ and hence satisfy $\omega(t) = \omega^*$ for all $t \geq 0$, and therefore $\dot{\omega}(t) = 0$ for all $t \geq 0$. We have, from (17), that

$$CP(t) \quad = \quad \left[\frac{\partial \Phi}{\partial \omega}(\omega(t))\right]^T \quad = \quad \left[\frac{\partial \Phi}{\partial \omega}(\omega^*)\right]^T \qquad \text{for all } t \geq 0. \tag{25}$$

Hence, the only trajectories $(\omega(t), P(t))$ in $\mathcal{Z}^+$ are those that satisfy $\omega(t) = \omega^*$ for all $t \geq 0$, and (25), i.e., they satisfy the KKT condition (19). Consequently, $\mathcal{Z}^+ \subseteq \mathcal{Z}^*$. ■

Remark 2. We make the following remarks regarding Theorem 4.

1) For a mesh network, $\mathcal{Z}^+$ is a strict subset of Z^*, because $\mathcal{Z}^+$ is compact, but $\mathcal{Z}^*$ is a subspace where there are uncountably many P^* that solves (21).
2) If we use the Lyapunov function in [14], then $\dot{U}(v) = 0$ if and only if $P^T C^T = \frac{\partial \Phi}{\partial \omega}(\omega)$, but not necessarily $\omega_i = \omega_j$. So each of these two Lyapunov functions enforces one of the two KKT conditions in (19). The proof for Theorem 4 can use either Lyapunov function.

Theorems 3 and 4 immediately imply that, for radial networks, the system converges to the unique saddle point.

Corollary 1. If $\mathcal{G}$ is a tree, every system trajectory $(d(t), \hat{d}(t), \omega(t), P(t))$ converges to the unique system optimal $(d^*, \hat{d}^*, \omega^*, P^*)$, i.e., it satisfies the three conclusions in Theorem 2.

Corollary 1 is a special case of Theorem 2 for radial networks. Convergence of the general networks requires a more careful argument because, for a mesh network, there is a subspace of saddle points in $\mathcal{Z}^*$ with the same ω^* but different P^* (Theorem 3). Theorem 4 only claims that $(\omega(t), P(t))$ approaches a compact subset of equilibrium points in $\mathcal{Z}^*$, but does not guarantee that it converges to a limit. We now show that it indeed does.

Consider $h(t) = CP(t)$, then (17)–(18) becomes

$$\dot{\omega} \quad = \quad \Gamma\left(\left[\frac{\partial \Phi}{\partial \omega}(\omega(t))\right]^T - h(t)\right), \tag{26}$$

$$\dot{h} \quad = \quad C\,\Xi\,C^T \omega(t). \tag{27}$$

By Lemma 2 in Section VII-B, a unique equilibrium point (ω^*, h^*) exists, which is globally asymptotically stable. Now we show that it is exponentially stable. Then, we will use the exponential stability of (ω^*, h^*) under dynamics (26)–(27) to conclude that $(\omega(t), P(t))$ itself converges to some limit point in $\mathcal{Z}^+$.

Theorem 5. Suppose the condition C1 is satisfied. Then, the equilibrium point (ω^*, h^*) of (26)–(27) is exponentially stable.

Proof: Since $\sum_{j \in \mathcal{V}} h_j(t) = 1^T CP(t) = 0$, where 1^T denotes the vector $[1 \ \cdots \ 1]$ of an appropriate dimension, we define $\tilde{h}(t) := [h_1(t) \ \cdots \ h_{N-1}(t)]^T$ as the first $N-1$ components of the vector $h(t)$. Let $\Delta\omega(t) := \omega(t) - \omega^*$ and $\Delta\tilde{h}(t) := \tilde{h}(t) - \tilde{h}^*$. Then (26)–(27) becomes, in terms of $\tilde{h}(t)$,

$$\Delta\dot{\omega} \quad = \quad \Gamma\left(\eta\left(\Delta\omega(t)\right) - A\,\Delta\tilde{h}(t)\right), \tag{28}$$

$$\Delta\dot{\tilde{h}} \quad = \quad \tilde{L}\,\Delta\omega(t), \tag{29}$$

where

$$\eta\left(\Delta\omega(t)\right) \quad := \quad \left[\frac{\partial \Phi}{\partial \omega}\left(\Delta\omega(t)+\omega^*\right) - \frac{\partial \Phi}{\partial \omega}\left(\omega^*\right)\right]^T \tag{30}$$

and $A := \begin{bmatrix} I \\ -1^T \end{bmatrix}$ is an $N \times (N-1)$ matrix with I being the $(N-1)\times(N-1)$ identity matrix. Here, $\tilde{L}$ is an $(N-1)\times N$ matrix obtained from the $N \times N$ weighted Laplacian matrix $C\,\Xi\,C^T$ by removing its last row. Then $\tilde{L}$ has a full row rank of $N-1$ [12]. The Jacobian matrix of (28)–(29) around the equilibrium $(\omega^*, \tilde{h}^*)$ is

$$\begin{bmatrix} -\Gamma\frac{\partial^2 \Phi}{\partial \omega^2}\left(\omega^*\right) & -\Gamma A \\ \tilde{L} & O \end{bmatrix},$$

which, by the condition C1, is bounded and Lipschitz. By [15, Thm. 3.13], (ω^*, h^*) is an exponentially stable equilibrium of (26)–(27) if and only if the origin is an exponentially stable equilibrium of the linear system

$$\frac{d}{dt}\begin{pmatrix} \Delta\omega \\ \Delta\tilde{h} \end{pmatrix} = \begin{bmatrix} -\Gamma\frac{\partial^2 \Phi}{\partial \omega^2}\left(\omega^*\right) & -\Gamma A \\ \tilde{L} & O \end{bmatrix}\begin{pmatrix} \Delta\omega \\ \Delta\tilde{h} \end{pmatrix}. \tag{31}$$

For all $j \in \mathcal{V}$ and all $l \in \mathcal{L}(j)$, let $\beta_l = d_l'(\omega^*)$. Consider the following *OLC* problem

$$\min_{d,\hat{d}} \qquad \sum_{j\in\mathcal{V}}\left(\sum_{l\in\mathcal{L}(j)}\frac{d_l^2}{2\beta_l} + \frac{1}{2D_j}\hat{d}_j^2\right) \tag{32}$$

$$\text{subject to} \qquad \sum_{j\in\mathcal{V}}\left(\sum_{l\in\mathcal{L}(j)} d_l + \hat{d}_j\right) = 0. \tag{33}$$

Following the techniques in Section III, we get a primal-dual algorithm to solve the *DOLC* and its dual problem corresponding to the *OLC* in (32)–(33). Such algorithm is described by the same linear system as in (31). By Lemma 2 in Section VII-B, the equilibrium of (31), which is the origin, is asymptotically stable, thus exponentially stable. Therefore, (ω^*, h^*) is an exponentially stable equilibrium of (26)–(27). ■

We now prove Theorem 2. By the global asysmptotic stability of (ω^*, h^*), $\omega(t) \to \omega^*$ as $t \to \infty$, where ω^* is the unique optimal of *DOLC*. By exponential stability of (ω^*, h^*), for all $(i,j) \in \mathcal{E}$, there exists some constant $\kappa_i > 0$, $\kappa_j > 0$, $\mu_i > 0$, $\mu_j > 0$, $\kappa_{ij} > 0$, $\mu_{ij} > 0$, and $t_0 \geq 0$, such that

$$\begin{aligned} |\omega_i(t) - \omega_j(t)| &\leq |\omega_i(t) - \omega^*| + |\omega_j(t) - \omega^*| \\ &\leq \kappa_i e^{-\mu_i(t-t_0)} + \kappa_j e^{-\mu_j(t-t_0)} \leq \kappa_{ij} e^{-\mu_{ij}(t-t_0)}, \end{aligned}$$

for all $t \geq t_0$. We first show that, for all $(i,j) \in \mathcal{E}$, $P_{ij}(t)$ satisfies the Cauchy condition: for any $\epsilon > 0$, there exists $T_\epsilon \geq t_0$, such that for all $s > t \geq T_\epsilon$, we have $|P_{ij}(s) - P_{ij}(t)| < \epsilon$. The proof is as follows. Note that for $t \geq t_0$,

$P_{ij}(t) = P_{ij}(t_0) + \xi_{ij} \int_{t_0}^{t} (\omega_i(\tau) - \omega_j(\tau))\, d\tau$, then

$$\begin{aligned}
|P_{ij}(s) - P_{ij}(t)| &= \left|\xi_{ij} \int_t^s (\omega_i(\tau) - \omega_j(\tau))\, d\tau\right| \\
&\leq \xi_{ij} \int_t^s |\omega_i(\tau) - \omega_j(\tau)|\, d\tau \\
&\leq \xi_{ij} \int_t^s \kappa_{ij} e^{-\mu_{ij}(\tau - t_0)} d\tau \\
&= \frac{\xi_{ij}\kappa_{ij} e^{\mu_{ij} t_0}}{\mu_{ij}} \left(1 - e^{-\mu_{ij}(s-t)}\right) e^{-\mu_{ij} t} \\
&< C_{ij}^0 e^{-\mu_{ij} T_\epsilon},
\end{aligned}$$

where $C_{ij}^0 = \frac{\xi_{ij}\kappa_{ij} e^{\mu_{ij} t_0}}{\mu_{ij}}$. Therefore, for any $\epsilon > 0$, we can find $T_\epsilon = \max\{\frac{\log(C_{ij}^0/\epsilon)}{\mu_{ij}}, t_0\}$, such that for all $s > t \geq T_\epsilon$, we have $|P_{ij}(s) - P_{ij}(t)| < \epsilon$.

Select any $\epsilon > 0$ and find T_ϵ. Let $\underline{P}_{ij} = \min\{\inf_{0 \leq \tau \leq T_\epsilon} P_{ij}(\tau), P_{ij}(T_\epsilon) - \epsilon\}$, and $\overline{P}_{ij} = \max\{\sup_{0 \leq \tau \leq T_\epsilon} P_{ij}(\tau), P_{ij}(T_\epsilon) + \epsilon\}$. It is easy to see that $\underline{P}_{ij} \leq P_{ij}(t) \leq \overline{P}_{ij}$, i.e., $P_{ij}(t)$ is bounded. Then, there exits a sequence $\{t_n,\ n \in \mathbb{N}\}$, where $t_0 < t_1 < \dots$, and a constant P_{ij}^*, such that $t_n \to \infty$ and $P_{ij}(t_n) \to P_{ij}^*$ as $n \to \infty$.

We now show that $\lim_{t\to\infty} P_{ij}(t) = P_{ij}^*$. By the convergence of the sequence $\{P_{ij}(t_n)\}$, for any $\epsilon > 0$, there exists $N\left(\frac{\epsilon}{2}\right) \in \mathbb{N}$, such that $\left|P_{ij}(t_n) - P_{ij}^*\right| < \frac{\epsilon}{2}$ for all $n \geq N\left(\frac{\epsilon}{2}\right)$. By the Cauchy condition, there exists $T_{\frac{\epsilon}{2}} \geq t_0$, such that for all $s > t \geq T_{\frac{\epsilon}{2}}$, we have $|P_{ij}(s) - P_{ij}(t)| < \frac{\epsilon}{2}$. Then, we can find $N'(\epsilon) \in \mathbb{N}$, such that $N'(\epsilon) \geq N\left(\frac{\epsilon}{2}\right)$ and $t_{N'(\epsilon)} \geq T_{\frac{\epsilon}{2}}$. For any $t \geq t_{N'(\epsilon)}$, and an arbitrarily selected $n \geq N'(\epsilon)$, we have

$$\begin{aligned}
|P_{ij}(t) - P_{ij}^*| &\leq |P_{ij}(t) - P_{ij}(t_n)| + \left|P_{ij}(t_n) - P_{ij}^*\right| \\
&< \frac{\epsilon}{2} + \frac{\epsilon}{2} = \epsilon.
\end{aligned}$$

By definition of convergence, $\lim_{t\to\infty} P_{ij}(t) = P_{ij}^*$.

Therefore, thre exists P^* , such that $\lim_{t\to\infty} P(t) = P^*$. Theorem 4 states that $(\omega(t), P(t))$ approaches a compact subset of equilibrium points in $\mathcal{Z}^*$, and now we have proved that it actually converges to a limit, which is primal-dual optimal for *DOLC* and its dual problem. By Theorem 1, we immediately get Theorem 2.

Remark 3. Regarding the convergence of $(\omega(t), P(t))$, we make the following additional remarks.

1) Standard application of LaSalle's invariance principle cannot conclude convergence because in our case $\mathcal{Z}^+$ contains multiple equilibrium points.
2) Even though none of the equilibrium points is asymptotically stable in the Lyapunov sense, any solution $(\omega(t), P(t))$ actually converges to one of the equilibrium points, the limit point depending on initial condition. This class of primal-dual algorithms go back to Arrow *et al.* [13] whose stability has been studied using a quadratic Lyapunov function, which we will also adopt (see below). See [14] for a recent stability analysis using a different Lyapunov function applied to constrained optimization.

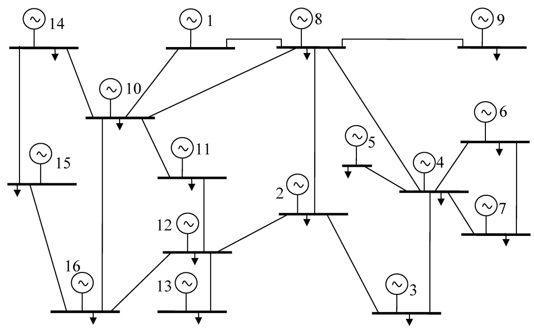

Fig. 2. The 16-generator transmission network model used in simulation. The arrows stand for controllable loads.

V. Case studies

To test the performance of the proposed *optimal load control (OLC)* mechanism, we run simulation on transmission network test beds built with MATLAB. As an example, we show simulation results on a 16-generator transmission network shown in Section V-A. In Sections V-B, a step change of mechanic power occurs at a subset of the buses, and the frequencies at different buses, the total change in load, and the objective value of *OLC* are observed. In Section V-C, the performance of *OLC* is compared with that of AGC, and the effect of their incorporation is also shown in simulation.

A. Transmission network model for simulation

We consider a 16-generator transmission network, which is a simplified version of the 16-generator, 68-bus and 86-transmission line test system of the New England/ New York interconnection given in [16]. We simplify the network in [16] by grouping a generator bus with its nearby load buses to form a bus with both generation and loads. Then, we get a 16-generator, 16-bus network, as shown in Figure 2. Note that some of the transmission lines in Figure 2 may be the equivalent of several parallel lines connecting different pairs of buses in the original network in [16], which are grouped as the same pair of buses in Figure 2.

The values of generator and transmission line parameters are taken from [17]. They, together with the values of parameters in *OLC*, are shown in Tables I and II. The reference voltage phase angle $\theta_j^0 = 0$ at all the buses. At bus j, $\underline{d} = \sum_{l\in\mathcal{L}(j)} \underline{d}_l$ and $\overline{d} = \sum_{l\in\mathcal{L}(j)} \overline{d}_l$ are respectively the lower bound and the upper bound on the total change in controllable loads. Every controllable load l has a cost function $c_l(d_l) = d_l^2/(2\alpha_l)$ on $d_l \in \left[\underline{d}_l, \overline{d}_l\right]$, where $\underline{d}_l < 0$ and $\overline{d}_l > 0$ are randomly generated subject to the bounds on total change in controllable loads, and $\alpha_l > 0$ is a random number. Here, we pick α_l uniformly distributed on $(0.2, 0.5)$.

In the model used for simulation, we relax some of the assumptions we made in previous sections. We consider non-zero line resistance and do not assume small differences between phase angle deviations. Moreover, at some of the buses, the damping constant $D_j = 0$, and at bus 1, there are no controllable loads. In practice, the frequency measurement and load control cannot be performed continuously in time. Therefore, in simulation, the loads measure

TABLE I

VALUES OF BUS PARAMETERS

Bus #	M_j (s)	D_j (pu)	$\|V_j\|$ (pu)	# loads	$\underline{d}$ (pu)	$\overline{d}$ (pu)
1	6.8000	0	1.045	0	0	0
2	9.8988	0	0.980	100	-3.14	3.14
3	9.9246	0	0.983	30	-0.82	0.82
4	8.3258	0	0 .997	30	-0.82	0.82
5	9.5334	0	1.011	70	-1.70	1.70
6	9.8214	0	1.050	30	-0.68	0.68
7	8.6534	0	1.063	60	-1.39	1.39
8	7.8300	0	1.030	100	-2.83	2.83
9	8.0730	0	1.025	50	-1.23	1.23
10	5.8212	0	1.010	40	-1.01	1.01
11	4.0106	0	1.000	10	-0.28	0.28
12	10.3582	0	1.016	80	-1.88	1.88
13	8.1564	4.0782	1.011	400	-16.34	16.34
14	6.0000	3.0000	1.000	150	-3.77	3.77
15	6.0000	3.0000	1.000	100	-2.88	2.88
16	8.9000	4.4500	1.000	300	-6.84	6.84

TABLE II

VALUES OF TRANSMISSION LINE PARAMETERS

From bus	To bus	r (pu)	x (pu)	From bus	To bus	r (pu)	x (pu)
1	8	0.0007	0.0086	8	9	0.0043	0.0474
1	10	0.0035	0.0411	8	10	0.0320	0.3200
2	3	0.0004	0.0050	10	11	0.0005	0.0047
2	8	0.0013	0.0213	10	14	0.0013	0.0188
2	12	0.0023	0.0363	10	16	0.0018	0.0274
3	4	0.0009	0.0094	11	12	0.0007	0.0085
4	5	0.0007	0.0138	12	13	0.0004	0.0040
4	6	0.0008	0.0135	12	16	0.0009	0.0221
4	7	0.0003	0.0059	14	15	0.0040	0.0600
4	8	0.0005	0.0056	15	16	0.0040	0.0600
6	7	0.0006	0.0096	-	-	-	-

the frequency and control their power every 250 ms. Moreover, the frequency measurements have Gaussian errors with a standard deviation of 3×10^{-5} pu (1.8 mHz) [18].

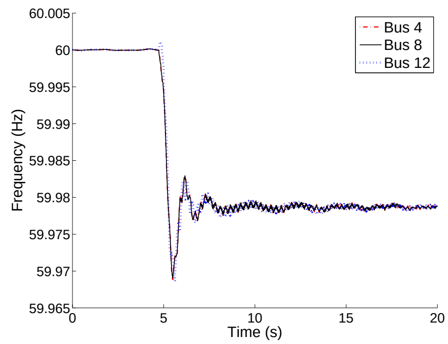

Fig. 3. Frequencies at buses 4, 8, 12, with loads performing *OLC*.

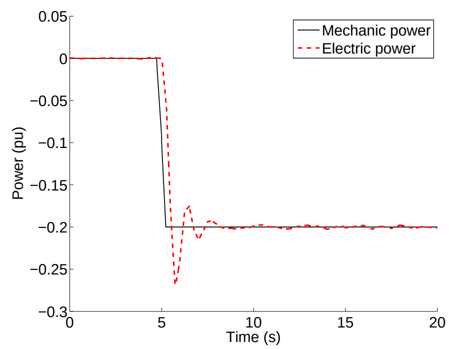

Fig. 4. Total change of mechanic power and electric power, with loads performing *OLC*.

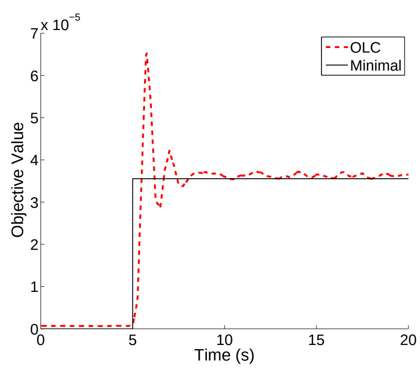

Fig. 5. Objective value of *OLC*.

B. Performane of OLC

At time $t = 5$ s, a step change of mechanic power occurs at buses 4, 8, 12. The controllable loads perform *OLC*. Figures 3, 4 and 5 respectively show the frequencies at buses 4, 8, 12, the total change in mechanic power and electric power, and the objective value of *OLC*. We see that that frequencies at three buses are driven to the

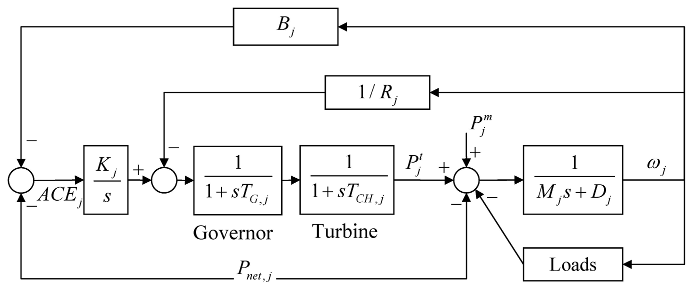

Fig. 6. Model of a bus equipped with AGC.

same value near 60 Hz, the total change in electric power balances the total change in mechanic power, and the objective value of *OLC* goes to the minimum, all in less than 5 seconds after the step change of mechanic power. In Figures 3–5, there are oscillations around the steady states, which may be caused by discrete-time load control or frequency measurement errors. The oscillations are relatively small compared to the steady state values. We see that the *OLC* has satisfactory performance in resynchronizing bus frequencies, matching load with generation and minimizing the aggregate disutility.

C. Incorporating OLC with AGC

AGC has been widely used in the regulation of transmission network. Hence, we compare the performance of *OLC* with AGC, and look at the effect of their incorporation.

The model of dynamics of bus j, equipped with AGC, is shown in Figure 6. In AGC, the generator controller computes area control error (ACE), which is a weighted sum of frequency deviation ω_j and the unscheduled net power flow out of the area $P_{net,j} = \sum_{k:j\to k} P_{jk} - \sum_{i:i\to j} P_{ij}$. The setpoint of the governor is adjusted according to the integral of ACE, and the change of mechanic power output of the turbine, P_j^t, is controlled by the governor. To improve stability, the governor also takes negative feedback of ω_j by the gain $1/R_j$. The governor and the turbine respectively have a time constant $T_{G,j}$ and $T_{CH,j}$. For all the generators in the simulation, we take $R_j = 0.1$ pu, $K_j = 0.05$, and $B_j = 1/R_j + D_j$ [9]. Moreover, for all the generators, $T_{G,j} = 0.04$ s, and $T_{CH,j} = 5$ s.

At time $t = 5$ s, a step change of mechanic power occurs at buses 4, 8, 12. Figures 7 and 8 respectively show the frequency at bus 12, and the total mismatch between electric power and mechanic power, in the case of using only AGC, using only *OLC* and incorporating both of them. Figures 7 and 8 show that, with AGC only, the frequency is driven to 60 Hz, and electric power and mechanic power are balanced in about 1 minute. However, within the first minute, there are large overshootings and oscillations in both frequency and electric-mechanic power mismatch. With *OLC* only, electric power and mechanic power are balanced in a short time, and the frequency is quickly driven to some value close to 60 Hz, but will not be driven to 60 Hz. When *OLC* is implemented together with AGC, the frequency can be driven to 60 Hz and electric power is balanced with mechanic power. Moreover, compared to the case of using AGC only, the settling time is decreased, and the overshooting in frequency and the

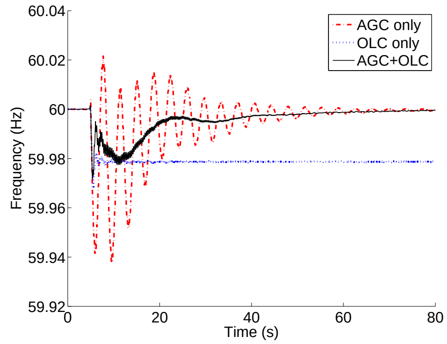

Fig. 7. Frequency at bus 12, with AGC only, with *OLC* only, or with both of them.

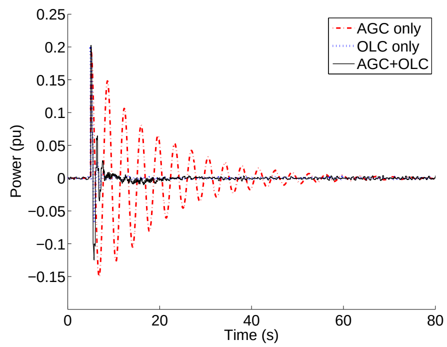

Fig. 8. Total mismatch between electric power and mechanic power, with AGC only, with *OLC* only, or with both of them.

oscillations in both frequency and electric-mechanic power mismatch are significantly alleviated. The result shows that adding *OLC* can improve the transient performance of AGC.

VI. Conclusion

We proposed an *optimal load control (OLC)* problem in power transmission networks. The objective of *OLC* is to minimize a measure of disutility of participation in load control, subject to the balance between total generation and load throughout the network. Then, we developed an equivalent problem of *OLC* through taking its dual problem, and designed a distributed primal-dual algorithm to solve that equivalent problem. The algorithm is composed by both the dynamics of the power network and a frequency-based load control mechanism. In the mechanism, loads are controlled as the inversed marginal disutility function of locally measured frequency. We proved that the trajectory produced by the algorithm convergences to the optimum of *OLC*. Simulation on a transmission network test bed showed that the proposed mechanism can resynchronize bus frequencies, balance load with generation and achieve the optimum of *OLC* within seconds after a disturbance in generation. Simulation also showed that adding *OLC* can improve the transient performance of AGC.

In practice, power transmission between buses may be limited due to the constraints on transmission line capacities. It would be a good extension to study the effect brought by line capacity constraints and develop control mechanism to ensure such constraints are satisfied. Moreover, voltage and reactive power regulation should be considered together with frequency and real power regulation. The incorporation of such two issues will produce a more realistic and complicated model which is interesting to investigate. We will also look into the distribution systems located under the transmission-level buses, and study the effect of load control when considering the distribution-level model together with the transmission-level model.

ACKNOWLEDGMENT

We thank Ross Baldick, David Chassin, Chris DeMarco, Ian Hiskens, and Kevin Tang for helpful discussions. We also thank Alec Brooks *et al.* from AeroVironment for their advice on practical issues. This work is supported by NSF NetSE grant CNS 0911041, ARPA-E grant DE-AR0000226, Southern California Edison, National Science Council of Taiwan R.O.C. grant NSC 101-3113-P-008-001, the Caltech Resnick Institute, and the Okawa Foundation.

VII. APPENDIX

A. *Proof of Theorem 1*

We first prove that *OLC* has a unique optimal point. Since c_l is continuous on $[\underline{d}_l, \overline{d}_l]$, $\sum_j \sum_{l\in\mathcal{L}(j)} c_l(d_l)$ is lower bounded, i.e., $\sum_j \sum_{l\in\mathcal{L}(j)} c_l(d_l) > \underline{C}$ for some $\underline{C}$. Let $(d', \hat{d}')$ be a feasible point (which exists by assumption C0). Let g denote the objective function of *OLC*. Then without loss of generality, we can constrain $\hat{d}$ to $\hat{d}_j^2 \le 2D_j(g(d', \hat{d}') - \underline{C})$ in *OLC*, because otherwise

$$g(d, \hat{d}) > \underline{C} + \frac{\hat{d}_j^2}{2D_j} > g(d', \hat{d}')$$

This makes the feasible set of *OLC* compact. Therefore there is a unique optimal point since g is continuous and strictly convex.

Since *OLC* has an objective function that is convex over $\mathbb{R}^k$, $k = N + \sum_j \sum_{l\in\mathcal{L}(j)} 1$, linear constraints, and a unique optimal $(d^*, \hat{d}^*)$, there is zero duality gap between *OLC* and *DOLC* and the dual optimal is attained at some ν^* [10, Proposition 5.2.1] [11]. Moreover, $d^* = d(\nu^*)$ given by (8) and $\hat{d}_j^* = D_j\nu^*$. We are left to prove that the dual optimal ν^* is unique.

Lemma 1. The objective function $\Phi(\nu) := \sum_j \Phi_j(\nu_j)$ of *DOLC* is strictly concave.

Proof: From (7), we have

$$\frac{\partial \Phi}{\partial \nu_j}(\nu) \quad = \quad \Phi_j'(\nu_j) \; = \; -\sum_{l\in\mathcal{L}(j)} d_l(\nu_j) - D_j\nu_j + P_j^m$$

Hence the Hessian of Φ is diagonal. Moreover, since $d_l(\nu_j)$ given by (8) is nondecreasing in ν_j, we have

$$\frac{\partial^2 \Phi}{\partial \nu_j^2}(\nu) \quad = \quad \Phi_j''(\nu_j) \; = \; -\sum_{l\in\mathcal{L}(j)} d_l'(\nu_j) - D_j \; < \; 0$$

Hence $\Phi(\nu)$ is strictly concave. ■

This proves that *DOLC* has a unique optimal ν^*. □

B. Global asymptotic stability of (ω^*, h^*)

Lemma 2. There is a globally asymptotically stable equilibrium (ω^*, h^*) of (26)–(27).

Proof: Since any solution $(\omega(t), P(t))$ approaches a subset of $\mathcal{Z}^*$ from any initial point $(\omega(0), P(0))$ (Theorem 4), and every point (ω, P) in $\mathcal{Z}^*$ has the same $\omega = \omega^*$ (Theorem 3), we have $\omega(t) \to \omega^*$ as $t \to \infty$ and $\dot{\omega} \to 0$. By the continuity of $\frac{\partial \Phi}{\partial \omega}(\omega)$, $\lim_t h(t) = \lim_t \frac{\partial \Phi}{\partial \omega}(\omega(t)) = \frac{\partial \Phi}{\partial \omega}(\omega^*) =: h^*$. Moreover (ω^*, h^*) is unique since ω^* is unique. Lemma 3 below implies that $(\omega(t), CP(t))$ is bounded starting from any initial point. Hence (ω^*, h^*) is globally asymptotically stable. ■

Lemma 3. Any solution $(\omega(t), P(t))$ of (17)–(18) is bounded for $t \geq 0$.

Proof: Recall the Lyapunov function $U(v)$. Since $\dot{U}(v(t)) \leq 0$, $\{v | U(v) \leq \alpha\}$ is compact and positively invariant with respect to (17)–(18) for any α. Moreover

$$U(v(t)) \;=\; \sum_{j \in \mathcal{V}} \frac{1}{2\gamma_j} \left(\omega_j(t) - \omega_j^*\right)^2 + \sum_{(i,k) \in \mathcal{E}} \frac{1}{2\xi_{ik}} \left(P_{ik}(t) - P_{ik}^*\right)^2 \;\leq\; U(z(0))$$

Therefore, for any particular j and all $t \geq 0$, we have

$$\frac{1}{2\gamma_j} \left(\omega_j(t) - \omega_j^*\right)^2 \leq U(v(t)) \leq U(v(0))$$

i.e., $\omega_j^* - \sqrt{2\gamma_j U(v(0))} \leq \omega_j(t) \leq \omega_j^* + \sqrt{2\gamma_j U(v(0))}$. Similarly, we have a bound on $P_{ik}(t)$ for any particular $(i,k) \in \mathcal{E}$ and all $t \geq 0$. ■

REFERENCES

[1] A. J. Wood and B. F. Wollenberg, *Power Generation, Operation, and Control*, 2nd Edition. NJ: John Wiley & Sons, Inc., 1996.

[2] M. Ilic and Q. Liu, "Toward sensing, communications and control architectures for frequency regulation in systems with highly variable resources," *Control and Optimization Theory for Electric Smart Grids*. New York: Springer, 2012.

[3] G. Heffner, C. Goldman, B. Kirby and M. Kintner-Meyer, "Loads providing ancillary services: Review of international experience," *Report of Lawrence Berkeley National Laboratory*, LBNL-62701, May 2007.

[4] A. Brooks, E. Liu, D. Reicher, C. Spirakis and B. Weihl, "Demand dispatch: Using real-time control of demand to help balance generation and load," *IEEE Power&Energy Magazine*, vol. 8, no. 3, pp. 21-30, 2010.

[5] B. Kirby, "Spinning Reserve From Responsive Loads," *Report of Oak Ridge National Laboratory*, ORNL/TM-2003/19, March 2003.

[6] A. Molina-Garcia, F. Bouffard and D. S. Kirschen, "Decentralized demand-side contribution to primary frequency control," *IEEE Trans. on Power Systems*, vol. 26, no. 1, pp. 411-419, 2001.

[7] M. Donnelly, D. Harvey, R. Munson and D. Trudnowski, "Frequency and stability control using decentralized intelligent loads: Benefits and pitfalls," in *Proc. of the 2010 IEEE Power and Energy Society General Meeting*, Minneapolis, MN, Jul. 2010.

[8] D. S. Callaway and I. A. Hiskens, "Achieving controllability of electric loads," *Proceedings of the IEEE*, vol. 99, no. 1, pp. 184-199, 2011.

[9] A. R. Bergen and V. Vittal, *Power Systems Analysis*, 2nd ed. Upper Saddle River, NJ: Prentice Hall, 2000.

[10] D. Bertsekas, *Nonlinear programming*, Athena Scientific, 1995

[11] S. Boyd and L. Vandenberghe, *Convex Optimization*, UK: Cambridge University Press, 2004.

[12] P. V. Mieghem, *Graph Spectra for Complex Networks*. UK: Cambridge University Press, 2011.

[13] K. Arrow, L. Hurwicz and H. Uzawa, *Studies in Linear and Non-Linear Programming*. CA, US: Stanford University Press, 1958.

[14] D. Feijer and F. Paganini, "Stability of primal-dual gradient dynamics and applications to network optimization," *Automatica*, 46(12), 2010, pp. 19741981.

[15] H. K. Khalil, *Nonlinear Systems*, 2nd Ed. NJ, US: Prentice-Hall, Inc., 1996.

[16] G. Rogers. *Power System Oscillations*. MA, US: Kluwer Academic Publishers, 2000.

[17] J. Chow and G. Rogers,*Power System Toolbox*, Version 3.0, 1991-2008.

[18] P. J. Douglass, R. Garcia-Valle, P. Nyeng, J. Ostergaard and M. Togeby, “Smart demand for frequency regulation: Experimental results,” *IEEE Transactions on Smart Grid*, 2012.